Ising systems with pairwise competing surface fields



2005 J. Phys.: Condens. Matter 17 6783

(http://iopscience.iop.org/0953-8984/17/43/001)

INSTITUTE OF PHYSICS PUBLISHING JOURNAL OF PHYSICS: CONDENSED MATTER

J. Phys.: Condens. Matter **17** (2005) 6783–6804 doi:10.1088/0953-8984/17/43/001

# Ising systems with pairwise competing surface fields

**A Milchev[1,2], A De Virgiliis[1] and K Binder[1]**

[1] Institut für Physik, Johannes Gutenberg-Universität, D-55099 Mainz, Staudinger Weg 7, Germany
[2] Institute for Physical Chemistry, Bulgarian Academy of Sciences, 1113 Sofia, Bulgaria

Received 9 August 2005, in final form 9 September 2005
Published 14 October 2005
Online at stacks.iop.org/JPhysCM/17/6783

**Abstract**

The magnetization distribution and phase behaviour of large but finite Ising simple cubic $L \times L \times L$ lattices in $d = 3$ dimensions and square $L \times L$ lattices in $d = 2$ dimensions are studied for the case where four free boundaries are present, at which surface fields $+H_s$ act on one pair of opposite boundaries while surface fields $-H_s$ act on the other pair (in $d = 3$, periodic boundary conditions are used for the remaining pair). Both the distribution $P_L(m)$ of the global magnetization and also the distribution of the local magnetization $m(x, z)$ are obtained by Monte Carlo simulations, where $x$ and $z$ denote the coordinates when the boundaries are oriented along the $x$-axis and $z$-axis (in $d = 2$); or along the $xy$-plane and $zy$-plane (in $d = 3$, where the periodic boundary condition applies in the $y$-direction). Varying the temperature $T$ and linear dimension $L$ it is found that a single bulk rounded phase transition occurs, which converges to the bulk transition temperature $T_{cb}$ as $L \to \infty$, unlike other geometric arrangements of competing boundary fields, where a second transition occurs in the bulk due to interface formation or delocalization, related to wedge or corner filling or wetting transitions, respectively. In the present geometry, only precursors of wetting layers form on those boundaries where the field is oppositely oriented to the magnetization in the bulk and the thickness of these layers is found to scale like $L^{1/2}$ (in $d = 2$) or $\ln L$ (in $d = 3$), respectively. These findings are explained in terms of a phenomenological theory based on the effective interface Hamiltonian and scaling considerations.

(Some figures in this article are in colour only in the electronic version)

## 1. Introduction

In recent years there has been much interest in clarifying wetting behaviour at flat surfaces as well as of systems exhibiting wedges and corners [1–23] and also the interplay of surface and interfacial phenomena with bulk phase transitions finds increasing attention [6, 24–37], in part motivated also by the fact that such phenomena may be relevant for devices of nanoscopic size,

  

as proposed for various purposes in nanotechnology. However, here we shall address only a very simple generic model, from the point of view of statistical thermodynamics, namely the nearest neighbour ferromagnetic Ising model on square and simple cubic lattices, with four free surfaces in both cases, at which competing boundary fields act (in the simple cubic case we apply a periodic boundary condition (p.b.c.) at the remaining two surfaces in the third direction).

When one applies competing boundary fields at two boundaries only ($+H_s$ on one boundary, $-H_s$ on the opposite boundary), choosing a p.b.c on the remaining two ($d = 2$) or four ($d = 3$) surfaces, one obtains the well studied case of the interface localization–delocalization transition [6, 24–30, 36, 37]. As is well known, the temperature at which this transition occurs tends to the wetting [1–6] transition temperature in the thermodynamic limit.

When one applies competing boundary fields at four boundaries such that two boundaries adjoining at a corner ($d = 2$) or a wedge ($d = 3$) get a field of the same sign, a different type of interface localization–delocalization transition occurs [31–35], related to the corner (wedge) filling transitions [7–23] of semi-infinite corners (or wedges, respectively). Note that in the thermodynamic limit the system undergoes 'bulk' transitions (in the sense that the total magnetization of the system changes, and/or that singularities of the total susceptibility, specific heat etc occur) at two distinct temperatures (cf figure 1): at the critical temperature $T_{cb}$ of the bulk Ising system, susceptibility and specific heat diverge, but the total magnetization remains zero, since domains of equal size but opposite orientation of the magnetization form. Only at a second (lower) transition temperature is the interface separating the two domains localized at one of the competing boundaries (in the interface localization transition related to the wetting transition, at the temperature $T_w$) [24–30] or at the corners (or wedges, respectively) [31–35], in the case of the interface localization transitions related to the filling transition, at the temperature $T_f$. We note that it depends on details of the model (such as whether exchange constants near the boundary are weaker or stronger than in the bulk, etc) whether these interface localization transitions are first order or (anomalous [31–35]) second order transitions. In the related case of a thin film with $L \times L \times D$ geometry and two competing $L \times L$ boundaries one may get sharp second order interface localization transitions in the limits $L \to \infty$ but $D$ finite also, of course, and these transitions belong to the $d = 2$ Ising universality class [6, 29, 30, 36, 37].

However, there exists a further possibility of arrangement of the boundary fields, namely, one may have the same sign of the field on opposite boundaries, so that the sign alternates as $+ - + -$ when one goes clockwise around the system. To the best of our knowledge, this possibility of boundary conditions has not yet been considered in the literature, and hence we fill this gap in the present paper. We show that, unlike the other choices of competing boundary fields, only a single transition affecting 'bulk' properties (bulk magnetization, susceptibility, etc) can now occur, and this transition takes place at $T_{cb}$. At $T_w$, wetting transitions occur at these boundaries where the sign of the boundary field is opposite to the sign of the bulk magnetization, but this transition implies a singularity of the surface free energy of the system only, and has no effect on any 'bulk' properties of the total system. Nevertheless, we are interested in analyzing the domain pattern that emerges as long as $L$ is still finite (figure 1(c)).

Of course, when one asks for experimental realizations of such systems, anisotropic magnets with competing surface fields may be difficult to produce in the laboratory. We note, however, that the Ising magnet may be re-interpreted as a lattice gas (spin up representing an empty cell and spin down an occupied cell), and the surface fields are related to particle-wall interactions (which may be repulsive or attractive, depending on the chemical nature of the wall). Similarly, the Ising magnet can also be mapped onto a lattice model for a binary (AB) mixture. It is clear that for such applications the condition of precise antisymmetry

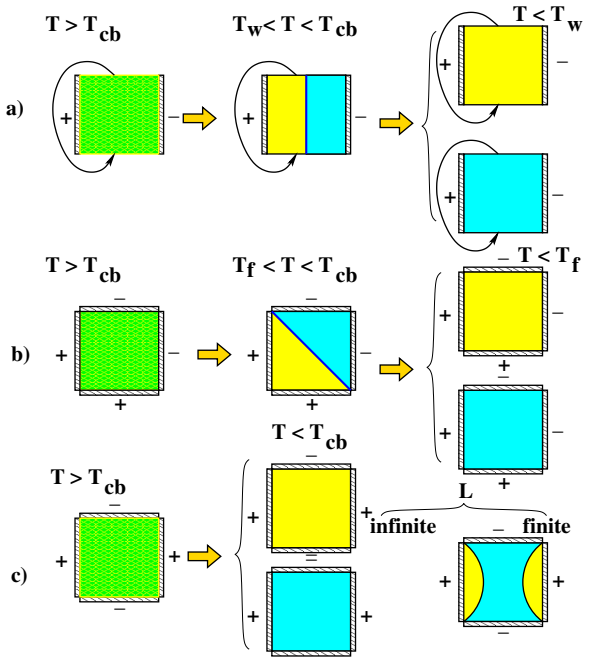


**Figure 1.** Schematic description of the phase transitions that occur in Ising $L \times L \times L$ cubes (or $L \times L$ squares, respectively) in the limit $L \to \infty$ for different choices of boundaries on which competing fields act. In case (a), there are only two free boundaries (shaded); at the remaining boundary (boundaries) periodic boundary conditions (p.b.c.) are applied, while in cases (b), (c) there are four free boundaries (shaded), and (in the case of dimensionality $d = 3$) a p.b.c. is applied in the third direction (perpendicular to the plane of the sketches). The sign of the competing surface fields $\pm H_s$ is indicated. Note that in cases (a) and (b) a phase transition occurs at the bulk transition temperature $T_{cb}$ towards a state with two domains of equal size but opposite orientation of magnetization, so the total magnetization remains zero for $T_w < T < T_{cb}$ (case a) or $T_f < T < T_{cb}$ (case (b)), respectively, $T_w$ and $T_f$ being the wetting and wedge filling transition temperatures, respectively. At the latter transition temperatures, the system obtains a spontaneous magnetization since the interface separating the equally sized domains moves to either the left or right wall (case (a)) or bottom left or top right wedge (corner), respectively (case (b)). In case (c), the transition to single-domain states already occurs at $T_{cb}$. However, for $T_w < T < T_{cb}$ one still has wetting layers on those walls whose surface field is oriented oppositely to the magnetization in the bulk, but the thickness $\ell_0$ of these wetting layers (though $\ell_0 \to \infty$) is negligible compared to $L$ in the thermodynamic limit.

of the boundary field is artificial, and one should consider the more general choice where the alternation of fields reads $+H_s$, $-H_s'$, $+H_s$, $-H_s'$. For simplicity, this complication is disregarded here and left for future work.

Our model, where along a square (or along a cube) different surface interactions occur, is an example of controlled nanoscale surface interactions, which have become of great interest in the context of nanotechnology as a means to influence the phase separation of polymer mixtures [38], the stability of thin adsorbed films [39] and their wetting behaviour [40]. The physics of nano-architectured and nano-structured materials in general is a rapidly developing field [41]. Although a simple Ising model study clearly is only a first step towards the description of the phase behaviour in such complicated real systems, we emphasize that Ising model studies of wetting, capillary condensation, interface localization, etc have become very fruitful to understand related phenomena for polymer mixtures, as exemplified in a recent

review [6]. We do expect that the interplay of interface free energies/surface excess free energies/line tensions that is crucial for the understanding of the phenomena in the present model, as is discussed below, will help to develop the insight with related phenomena for more complex materials influenced by controlled nanoscale interactions.

The outline of the present paper is as follows. In the next section, we describe a simple phenomenological theory based on the concept of the effective interface Hamiltonian [1–6] and on the scaling theory of surface critical phenomena [42–44]. In section 3, we present our Monte Carlo results for the case $d = 3$, and in section 4 for the case $d = 2$. Section 5 gives a summary and outlook for further work.

## 2. Phenomenological theory

In this section we consider Ising square ($L \times L$) or simple cubic ($L \times L \times L$) lattices with free boundaries at which pairwise competing fields $\pm H_s$ act, as shown in figure 1(c). In the absence of a bulk field $H$, no sign of the total magnetization is preferred by the system. We are interested in how in a finite system the transition takes place from the disordered phase for $T > T_{cb}$ over a state with a strongly inhomogeneous distribution of the magnetization in the critical region (figure 2) to a state where the system basically is in a monodomain configuration, but 'decorated' with precursors of wetting layers at these boundaries where the sign of the surface field is opposite to the sign of the magnetization, at temperatures well below $T_{cb}$.

In the different regimes of temperature, different theoretical approaches are applied. While for temperatures in the critical region we rely on phenomenological scaling descriptions [42, 43], for temperatures well below $T_{cb}$ (where the correlation length in the bulk and hence the 'intrinsic thickness' of the interface is of the order of the lattice spacing [45–48]) we apply the concept of the effective interface Hamiltonian [1–6]

$$\mathcal{H}_{\text{eff}}\{\ell\} = \int \mathrm{d}x \left[ \frac{\sigma}{2} \left( \frac{\mathrm{d}\ell}{\mathrm{d}x} \right)^2 + V_{\text{eff}}(\ell) \right], \tag{1}$$

where $\sigma$ is the interfacial stiffness, and $V_{\text{eff}}(\ell)$ the effective potential caused by the boundary field. In the simplest case of short range forces caused by the boundary, as is implied by boundary fields $\pm H_s$ acting on the surface plane (or surface row, in the $d = 2$ case, respectively), at temperatures $T$ higher than the wetting transition temperatures $T_w$, one may take [1–6, 29]

$$V_{\text{eff}} = a \exp(-\kappa \ell), \qquad a > 0, \tag{2}$$

$\kappa^{-1}$ being a decay length which is of the order of the correlation length of order parameter fluctuations in the bulk.

Note that by equations (1) and (2) we have tacitly omitted any contributions due to the line tension [46, 49–53], i.e. the free energy excess due to the contact line (in $d = 3$) where the interface between domains of up spins and down spins meets the edge (figure 2). This neglect is motivated simply by the lack of knowledge of the line tension for the chosen geometry. However, assuming that for small contact angles of the interface the line tension should not depend on the contact angle, the line tension anyway should not affect the analysis which follows.

We are now interested in deriving the function $\ell(x)$ that describes the local distance of the interface from the boundary (figure 2). This function can be found from the consideration that $\mathcal{H}_{\text{eff}}\{\ell(x)\}$ can be interpreted as a free energy functional that one wishes to minimize, subject to the boundary conditions

$$\mathcal{H}_{\text{eff}}\{\ell(x)\} \to 0, \qquad \ell(x = \pm L/2) = 0. \tag{3}$$

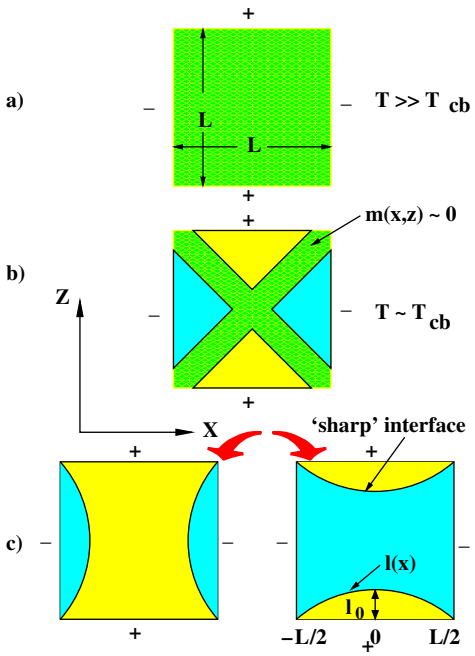


**Figure 2.** Schematic description of the change of state in case (c) of figure 1 for the case where the linear dimension $L$ is large but finite. Far above $T_c$ (a) the system is basically disordered everywhere (only on a scale of the correlation length $\xi_b$ the boundary fields induce a weak local order close to the respective boundaries (not shown)). Near $T_{cb}$, however, when $\xi_b$ has grown to a size comparable to $L$, the order induced by the surface fields has spread out to domains that range almost towards the center of the system (but the magnetization $m(x, y)$ in these domains is strongly inhomogeneous and decreases smoothly to zero when the interfacial regions (shaded) are reached; of course, there are no sharp interfaces, since the interfacial width is of the same order as $\xi_b$, when one is below $T_{cb}$). From this state, the system can develop to either the left or the right domain configuration when the system is cooled further to a temperature far enough below $T_{cb}$ (but above the temperature $T_w(H_s)$) such that $\xi_b \ll L$ (case (c)). Then precursors of wetting layers are separated from the majority domain by a 'sharp' interface (i.e., its 'intrinsic' thickness is of order $\xi_b$) with average location at $\ell(x)$.

This leads to the Euler–Lagrange equation

$$\frac{dV_{\text{eff}}}{d\ell} = -\kappa a \exp(-\kappa\ell) = \sigma \frac{d^2\ell}{dx^2}. \tag{4}$$

This nonlinear ordinary differential equation is readily solved, noting the analogy with classical mechanics: interpreting $x$ as a time variable $t$, $\ell$ as a spatial coordinate $y$, the equation $\sigma\, d^2y/dt^2 = -\kappa a \exp(-\kappa y)$ is Newton's law of classical mechanics, which is readily integrated once using energy conservation: multiplying by $\dot{y} = dy/dt$, the resulting equation is $(d/dt)[-a\exp(-\kappa y) + \sigma\dot{y}/2] = dE/dt = 0$. The energy $E$ must be chosen such that the kinetic energy is zero on the 'top of the hill', i.e. for $y = \ell_0$. So we must choose $E = -a\exp(-\kappa y) + \sigma\dot{y}^2/2 = -a\exp(-\kappa\ell_0)$. The 'particle' starts with maximum velocity at the point $y = 0$ and rolls up to the point $y = \ell_0$, where it slows down to zero velocity. So the result of this consideration is, translated back to our problem,

$$(\sigma/2a)(d\ell/dx)^2 = \exp(-\kappa\ell) - \exp(-\kappa\ell_0), \qquad 0 \leqslant \ell \leqslant \ell_0. \tag{5}$$

This differential equation can be solved by simple quadrature,

$$x = \pm\sqrt{\frac{\sigma}{2a}}\int_{\ell}^{\ell_0}\frac{\mathrm{d}\ell'}{\sqrt{\exp(-\kappa\ell') - \exp(-\kappa\ell_0)}} + \text{const}, \tag{6}$$

and substituting $y = \exp(-\kappa\ell)$ we find the solution in terms of an elementary integral $[y_0 = \exp(-\kappa\ell_0)]$

$$\sqrt{\frac{2a}{\sigma}}\kappa x = \pm\int^{y}\frac{\mathrm{d}y'}{y'\sqrt{y'-y_0}} + \text{const} = \pm\frac{2}{\sqrt{y}}\arctan\sqrt{\frac{y-y_0}{y_0}} + \text{const}. \tag{7}$$

Noting that $x = 0$ corresponds to $\ell = \ell_0$, and $\arctan 0 = 0$, we find that the integration constant is zero, and hence

$$\sqrt{\frac{2a}{\sigma}}\exp(-\kappa\ell_0)\frac{\kappa x}{2} = \arctan\sqrt{\exp(-\kappa(\ell-\ell_0)] - 1}, \tag{8}$$

which is readily inverted as

$$\kappa[\ell(x) - \ell_0] = 2\ln\left\{\cos\left[\sqrt{\frac{2a}{\sigma}}\exp\left(-\frac{\kappa\ell_0}{2}\right)\frac{\kappa x}{2}\right]\right\}. \tag{9}$$

The condition that $\ell(x = \pm L/2) = 0$ fixes $\ell_0$, in terms of the transcendental equation

$$\exp(\kappa\ell_0) = 1 + \tan^2\left[\sqrt{\frac{2a}{\sigma}}\exp\left(-\frac{\kappa\ell_0}{2}\right)\frac{\kappa L}{4}\right]. \tag{10}$$

Since for $L \to \infty$ we also have $\ell_0 \to \infty$ (for $T > T_{\mathrm{w}}$, as assumed here through our choice for $V_{\mathrm{eff}}(\ell)$), the argument of the tan-function must go to $\pi/2$ for $L \to \infty$. This yields

$$\ell_0 = \frac{2}{\kappa}\ln\left(\frac{\kappa L}{2\pi}\sqrt{\frac{2a}{\sigma}}\right). \tag{11}$$

A logarithmic growth of wetting layers in finite systems (but for periodic boundary conditions, such that $\ell(x) \equiv \tilde{\ell}_0$ throughout) has already been obtained in early work by Kroll and Gompper [54].

It is also interesting to generalize this treatment to long range forces at the boundaries, such as an effective potential decaying as a power law,

$$V_{\mathrm{eff}}(\ell) = a\ell^{-p}, \qquad \ell \to \infty. \tag{12}$$

A reasoning analogous to the arguments leading from equations (3) to (5) now yields

$$\frac{\sigma}{2a}\left(\frac{\mathrm{d}\ell}{\mathrm{d}x}\right)^2 = \ell^{-p} - \ell_0^{-p}, \qquad a_0 \leqslant \ell \leqslant \ell_0, \tag{13}$$

where we have replaced the lower limit zero in equation (5) by the lattice spacing $a_0$ to cut off the divergence of the potential, equation (12), as $\ell \to 0$. The result analogous to equation (6) reads

$$x = \pm\sqrt{\frac{\sigma}{2a}}\int_{\ell}^{\ell_0}\mathrm{d}\ell'/\sqrt{\ell'^{-p} - \ell_0^{-p}}. \tag{14}$$

Since we are not aware of a simple solution of the integral in equation (14) in terms of elementary functions, we consider various approximations. Near $x = \pm L/2$, where $\ell$ is close to its lower limit $a_0$, the term $\ell_0^{-(p+1)}$ is negligible in comparison with $\ell^{-(p+1)}$ in equation (13). Hence we obtain, for $x > 0$

$$L/2 - x = \sqrt{\frac{\sigma}{2a}}\int_{a_0}^{\ell}\mathrm{d}\ell'(\ell')^{p/2} = \sqrt{\frac{\sigma}{2a}}\frac{(\ell - a_0)^{(p/2+1)}}{(p/2+1)}. \tag{15}$$

An analogous solution can easily be written down for $x < 0$. If one could use equation (15) even for $x = 0$, one would conclude

$$L/2 \approx \sqrt{\frac{\sigma}{2a}}\,\frac{\ell_0^{(p/2+1)}}{(p/2+1)}, \qquad \ell_0 \approx (2a/\sigma)^{1/(p+2)}\left[\frac{(p+2)}{4}L\right]^{2/(p+2)}. \tag{16}$$

An approximate solution with the right symmetry properties with respect to the sign of $x$ then reads, for $\ell(x) \gg a_0$,

$$\ell(x) = \left[\frac{2a}{\sigma}\left(\frac{p+2}{4}\right)^2\right]^{\frac{1}{p+2}} \left\{\left(\frac{L}{2}-x\right)^{2/(p+2)} + \left(\frac{L}{2}+x\right)^{2/(p+2)} - L^{2/(p+2)}\right\} \Big/ \left(2^{\frac{p}{p+2}}-1\right). \tag{17}$$

Equation (17) reduces to equation (16) for $x = 0$ and satisfies the condition $\ell(x = \pm L/2) = 0$, although near $x = L/2$ equation (15) is not strictly satisfied.

Fortunately, (14) can be expressed in terms of elementary functions for some special cases of physical interest, such as $p = 1$ and $p = 2$. In the latter case the solution is particularly simple, the shape of the interface is an ellipse,

$$[\ell(x)]^2 = \sqrt{\frac{a}{2\sigma}}L\left(1 - \frac{4x^2}{L^2}\right), \qquad \ell_0 = \left(\frac{a}{2\sigma}\right)^{1/4}\sqrt{L}, \tag{18}$$

while for $p = 1$ we find

$$\sqrt{\frac{2a}{\sigma}}x = -\sqrt{\ell_0\ell(\ell_0-\ell)} + \ell_0^{3/2}\left(\arctan\sqrt{\frac{\ell}{\ell_0-\ell}} - \frac{\pi}{2}\right), \qquad \ell_0 = \left(\frac{2a}{\pi^2\sigma}\right)^{1/3} L^{2/3}. \tag{19}$$

From these results one sees that the simple approximation (16) predicts correctly the exponent of $L$ but overestimates the prefactor.

A particularly interesting case occurs for $d = 2$ and short range boundary fields: as emphasized by Fisher [55], the one-dimensional interface can be viewed at low temperatures as a random walk problem, interpreting $x$ as a time variable, and with probability $p \ll 1$ a step occurs either in the $+y$-direction or in the $-y$-direction (and with probability $1-2p$ the walker continues in the $x$-direction). Due to the condition $p \ll 1$, which holds at low temperatures, no overhangs occur in the interfacial configurations, and then this mapping between Ising interfaces in two-dimensional ferromagnets and random walks becomes exact. From the analysis presented by Fisher [55] one can conclude that the effect of statistical fluctuations of such an interface interacting with a repulsive wall at $y = 0$ can be described by a mean-field treatment of the Hamiltonian equation (1) with an effective entropic potential

$$V_{\mathrm{eff}}(\ell) \approx \frac{1}{2}k_{\mathrm{B}}T\,\frac{d_0^2}{\ell^2}, \qquad \ell \gg a_0. \tag{20}$$

From this random walk picture, Fisher also shows that for a bubble of basis length $L$ (i.e., an interface touches an infinite wall at $x = -L/2$ and then again at $x = L/2$, but these points are not special points of the wall, which continues straight on both to $x \to -\infty$ and to $x \to +\infty$ at $y = 0$), one obtains an elliptical shape, with a small axis of the ellipse scaling as $\ell_0 \propto \sqrt{L}$. Although this is not precisely our problem—here the points $x = \pm L/2$ are special, due to the boundaries along the $y$-direction that join there—it is interesting that for $p = 2$ (corresponding to equation (20)) the approximate equation (17) is just such an elliptical shape of the interface as found by Fisher [55].

All the above considerations are applicable only in an intermediate temperature regime, for temperatures sufficiently far below the bulk critical temperature $T_{\mathrm{cb}}$ (such that the correlation length $\xi_{\mathrm{b}}$ is much less than $L$), but above the wetting transition temperature $T_{\mathrm{w}}(H_{\mathrm{s}})$. Near $T_{\mathrm{cb}}$

a treatment in terms of the capillary wave Hamiltonian considered within mean-field theory is inappropriate, of course, when $\ell_0$ is no longer much larger than $\xi_b$. In this regime, however, some conclusions are possible from the general scaling theory of surface critical phenomena [42–44]. Noting that $\xi_b \propto |t|^{-\nu}$ where $t = 1 - T/T_{cb}$ and $\nu \approx 0.63$ is the correlation length critical exponent in the Ising universality class [56–58], the singular part of the free energy can be written in terms of a scaling function $\tilde{f}_\pm$,

$$f_{sing}(T, H, H_s, L) = |t|^{2-\alpha} \tilde{f}_\pm(L|t|^\nu, H|t|^{-\Delta}, H_s|t|^{-\Delta_1}). \tag{21}$$

Here we have included a bulk magnetic field $H$, $\alpha \approx 0.110$ is the critical exponent of the bulk specific heat [57, 58], $\Delta = \beta + \gamma = 1.564$ [57, 58] ($\beta$, $\gamma$ being the exponents of the bulk order parameter and susceptibility, respectively), while $\Delta_1 \approx 0.47 \pm 0.01$ is the new exponent describing the surface critical behaviour [42–44]. In $d = 2$ dimensions, however, all these critical exponents are exactly known [42–44, 56–58], namely $\alpha = 0$, $\nu = 1$, $\Delta = 15/8$, and $\Delta_1 = 1/2$).

Taking derivatives with respect to the bulk field one can also write down analogous relations for the magnetization $m$ and susceptibility $\chi$,

$$m = -\left(\frac{\partial f_{sing}}{\partial H}\right)_{T,H_s} = |t|^\beta \tilde{m}_\pm(L|t|^\nu, H|t|^{-\Delta}, H_s|t|^{-\Delta_1}), \tag{22}$$

$$\chi = -\left(\frac{\partial^2 f_{sing}}{\partial H^2}\right)_{T,H_s} = |t|^{-\gamma} \tilde{\chi}_\pm(L|t|^\nu, H|t|^{-\Delta}, H_s|t|^{-\Delta_1}), \tag{23}$$

where the scaling relation $2 - \alpha = \gamma + 2\beta$ [56] was used, and $\tilde{m}_\pm$, $\tilde{\chi}_\pm$ are scaling functions resulting from the derivative of $\tilde{f}_\pm$. It is often convenient to rewrite these scaling functions in terms of other variables, namely using $X \equiv L^{1/\nu}t$ to eliminate all other powers of $|t|$ by powers of $L$,

$$\chi = L^{\gamma/\nu} \tilde{\chi}(L^{1/\nu}t, HL^{\Delta/\nu}, H_s L^{\Delta_1/\nu}), \tag{24}$$

$$\langle m \rangle = L^{-\beta/\nu} \tilde{m}(L^{1/\nu}t, HL^{\Delta/\nu}, H_s L^{\Delta_1/\nu}). \tag{25}$$

Equations (24) and (25) are particularly convenient for finite size scaling analysis, since at fixed $L$ the new scaling functions $\tilde{\chi}$ and $\tilde{m}$ are analytic functions of $t$, $H$ and $H_s$ also at $T_{cb}$. Nevertheless, since the scaling functions still contain three arguments, a complete test of finite size scaling in terms of all three variables is rather demanding. Thus, we shall focus on interesting special cases only. For example, choosing $t = 0$ (i.e., $T = T_{cb}$) and $H = 0$, one finds that the second moment of the magnetization distribution scales as

$$\langle m^2 \rangle L^{2\beta/\nu} = \tilde{m}_2(0, 0, H_s L^{\Delta_1/\nu}), \tag{26}$$

so one can check data collapse on a function of a single scaling variable $H_s L^{\Delta_1/\nu}$ then. It is also interesting to locate in the plane of variables ($t$, $H = 0$, $H_1$) the curve where the susceptibility has its maximum, since the condition $d\chi/dt = 0$ leads to

$$\tilde{\chi}^{(1)}(L^{1/\nu}t, O, H_s L^{\Delta_1/\nu}) = 0 \tag{27}$$

where $\tilde{\chi}^{(1)}$ is the derivative of the scaling function of the susceptibility $\chi'$, with respect to its first argument $X$, and $\chi'$ is defined as

$$k_B T \chi' = L^d(\langle m^2 \rangle - \langle |m| \rangle^2), \tag{28}$$

$d$ being the dimensionality of the system. Here we recall that finite size scaling implies that the hyperscaling relation [56] $d\nu = \gamma + 2\beta$ holds, and that in finite systems the susceptibility $\chi'$ that converges to the proper result in the limit $L \to \infty$ for $H = 0$ needs to use the absolute value $\langle |m| \rangle$ rather than $\langle m \rangle$ [59] because in the finite systems there is no broken symmetry, and hence $\langle m \rangle \equiv 0$ for $H = 0$.

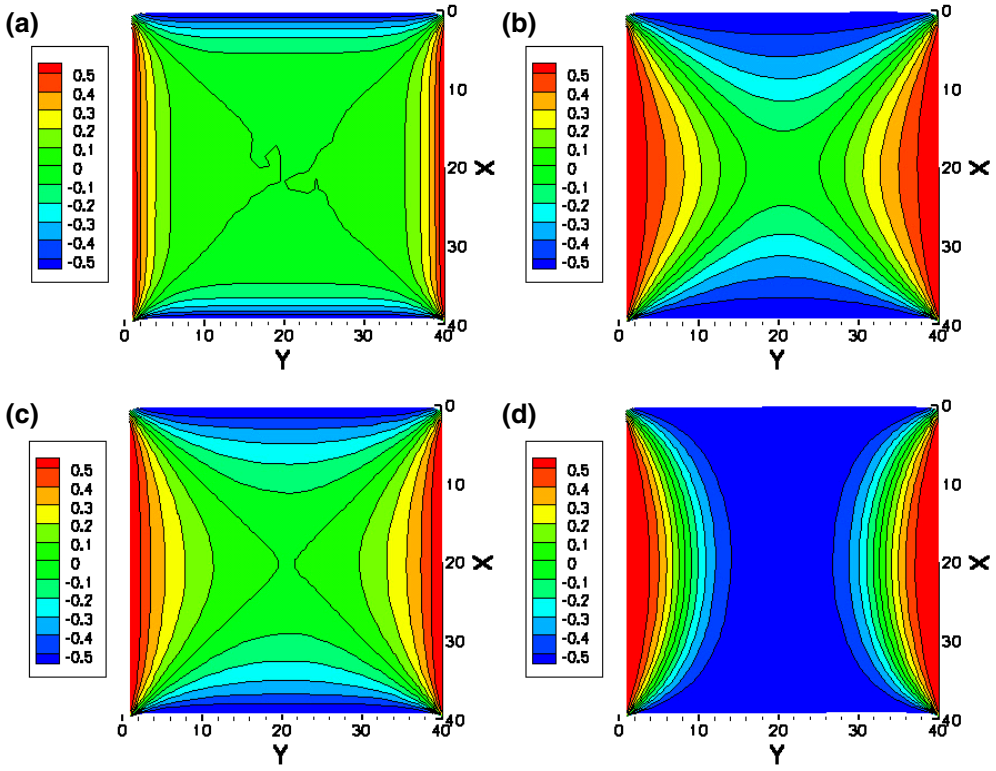


**Figure 3.** Contour diagram of the magnetization distribution for $L = 40$, $H_s = -2$ and four choices of $\beta = J/k_BT$, $\beta = 0.208$ (a), 0.220 (b), 0.226 (c), and 0.232 (d). The key for the colour coding is included. All data are based on averages over $2 \times 10^5$ Monte Carlo steps (MCSs) per spin. Note that the coordinates are denoted as $X$ and $Y$ here (rather than $x$ and $z$) and run from 0 to $L$.

## 3. Monte Carlo results: the three-dimensional case

We have carried out Monte Carlo simulations for the simple cubic nearest neighbour Ising ferromagnet, varying $L$ typically from $L = 20$ up to 100 (occasionally also smaller values, such as $L = 10$, and larger values, such as $L = 160$, are included) and also varying both the inverse temperature $\beta = J/k_BT$ and the surface field $H_s/J$, but choose $H = 0$ throughout. We measure here all lengths in units of the lattice spacing, and also choose $J \equiv 1$. The standard Metropolis algorithm is used (due to our choice of surface fields the use of cluster algorithms [60] would offer hardly any advantage [61]).

Figures 3 and 4 show typical results for $L = 40$ in terms of contour diagrams of the magnetization. The case of figure 3(a) illustrates the precise structure of the disordered state (figure 2(a)): there is a nonzero magnetization near all the surfaces, where the boundary fields act, but this magnetization decays towards zero after a few lattice spacings as one moves towards the bulk, and in most of the system the magnetization is close to zero. On the other hand, for cases (b) and (c), we recognize almost triangular-like cross-sections of the regions where the magnetization is distinctly nonzero, and the corresponding configuration of a St Andrew's cross of the interfacial region, where $m(x, z) \approx 0$ (figure 2(b)). The lowest temperature (figure 3(d)) exhibits a state where the average magnetization in the system is nonzero, namely negative,

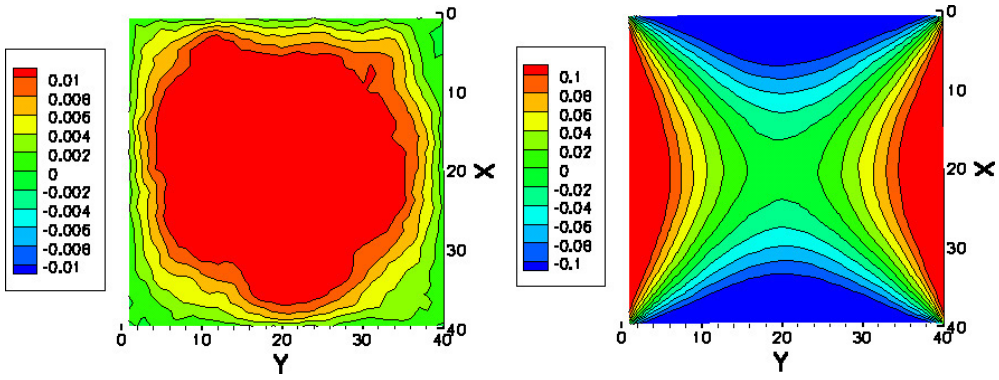


**Figure 4.** The same as figure 3, but choosing for $\beta$ the value at the critical point ($\beta_c \approx 0.2217$ [60]) and $H_s = 0$ (left part) or $H_s = -0.3$ (right part). Note the different range of the scale of the colour coding in both figures.

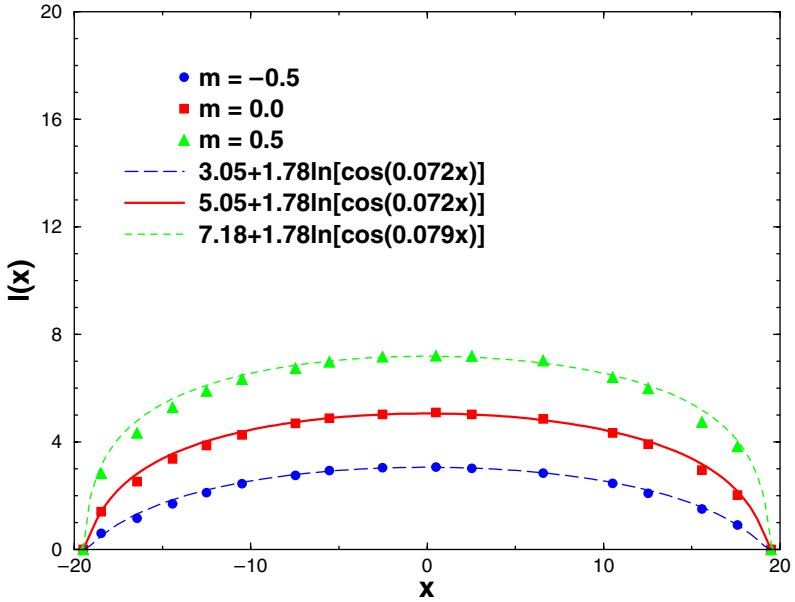


**Figure 5.** Contours $m(x, z) = 0.5$, $m(x, z) =$ and $m(x, z) = -5$ near the surface at $z = 0$ for the case $L = 40$, $\beta = 0.25$, $H_s = -2$. The contour for $m = 0$ is compared to a fit to equation (9). Note that due to statistical fluctuations the isolines are not strictly symmetric around the line $x = 20$ in this plot (again $2 \times 10^5$ MCSs were used).

unlike the other three contour plots shown, which still exhibit the full symmetry of a system which has average magnetization $\langle m \rangle = 0$. This is an example of the situation envisaged in figure 2(d).

The magnitude of the surface field chosen in figure 3 is rather strong. Therefore, we examine what happens for other choices of the field $H_s$ (figure 4). We see that for $H_s = 0.3$ the behaviour is qualitatively still the same for the choice $H_s = 2.0$ in the critical region. A different behaviour, however, is expected for very weak fields, because then the magnetization in the surface layers may still be weakened due to the 'missing neighbour'-effect of the free surfaces,

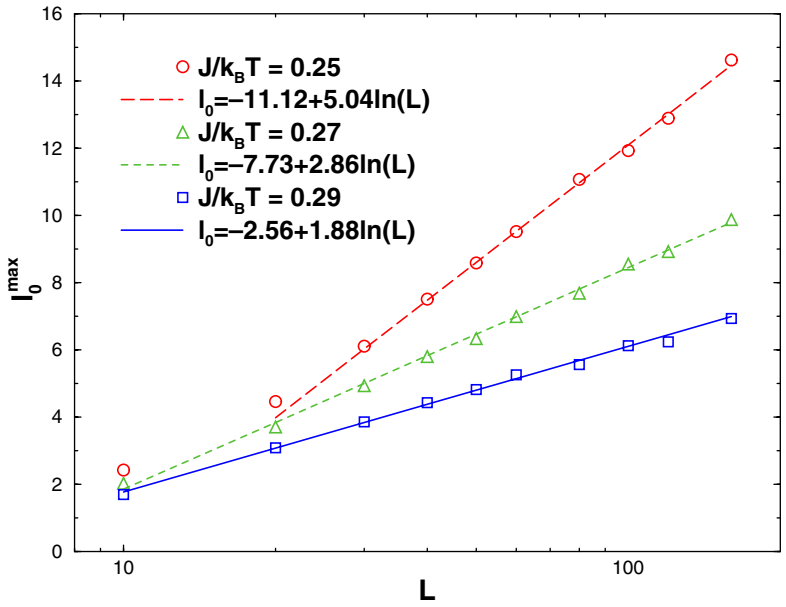


**Figure 6.** Plot of $\ell_0$ versus $L$ (note the logarithmic scale of the abscissa) for three inverse temperatures $\beta = 0.25$, 0.27 and 0.29, using $H_s = -2$ and box linear dimensions ranging from $L = 10$ to $L = 160$. Straight lines show fits to equation (11). Parameters of the fit are quoted in the figure.

at least for $T < T_{cb}$. At $T = T_{cb}$ and for $H_s = 0$, the fluctuations of the magnetization are reduced (this is known [42–44] from the study of critical correlations near surfaces, of course). In our case this is reflected by the fact that the average magnetization in the bulk, which is not strictly zero when an average over a finite observation time is taken, because of the magnetization fluctuations, is still of order 0.01 in the bulk while it is only of order 0.002 in the surface region (figure 4, left part).

Figure 5 presents then a quantitative comparison of the isolines of the magnetization with the theory of section 2. Of course, the phenomenological interface Hamiltonian, equation (1), treats the interface as a sharp kink at $z = \ell(x)$ where the local magnetization $m(x, z)$ exhibits a jump from $-m_b$ to $+m_b$ (or vice versa), $m_b$ being the bulk magnetization of an infinite ferromagnet at the same temperature. It is clear from figure 3(d), however, that the transition from $-m_b$ to $+m_b$ is rather gradual, and spread out over several lattice spacings, and this fact also remains true at lower temperature, such as $k_B T/J = 4$ shown in figure 5. In this case $m_b \approx 0.75$ and $\xi_b$ is less than two lattice spacings [27]. The distances (in the $y$-direction) between the isolines at $m = -0.5$, 0, +0.5 are somewhat larger than $\xi_b$, however. This fact already indicates some broadening of the interfacial profiles due to additional statistical fluctuations, presumably capillary waves [45–48]. Similar interfacial broadening through capillary waves has been found from simulations in other geometries as well [6, 27–36]. In spite of these deviations from the simple description of the interface as a sharp kink in a potential, treated in a mean-field approximation, equation (9) yields a fair description of the average interface position, if the contour $m(x, z) = 0$ is identified with the contour $z = \ell(x)$. Of course, systematic deviations near the corners of the cube, where $\ell(x) \to 0$, must be expected, and do occur.

Figure 6 then shows a test of equation (11). It is seen that for all three temperatures the predicted logarithmic variation is compatible with the simulation data in the range from

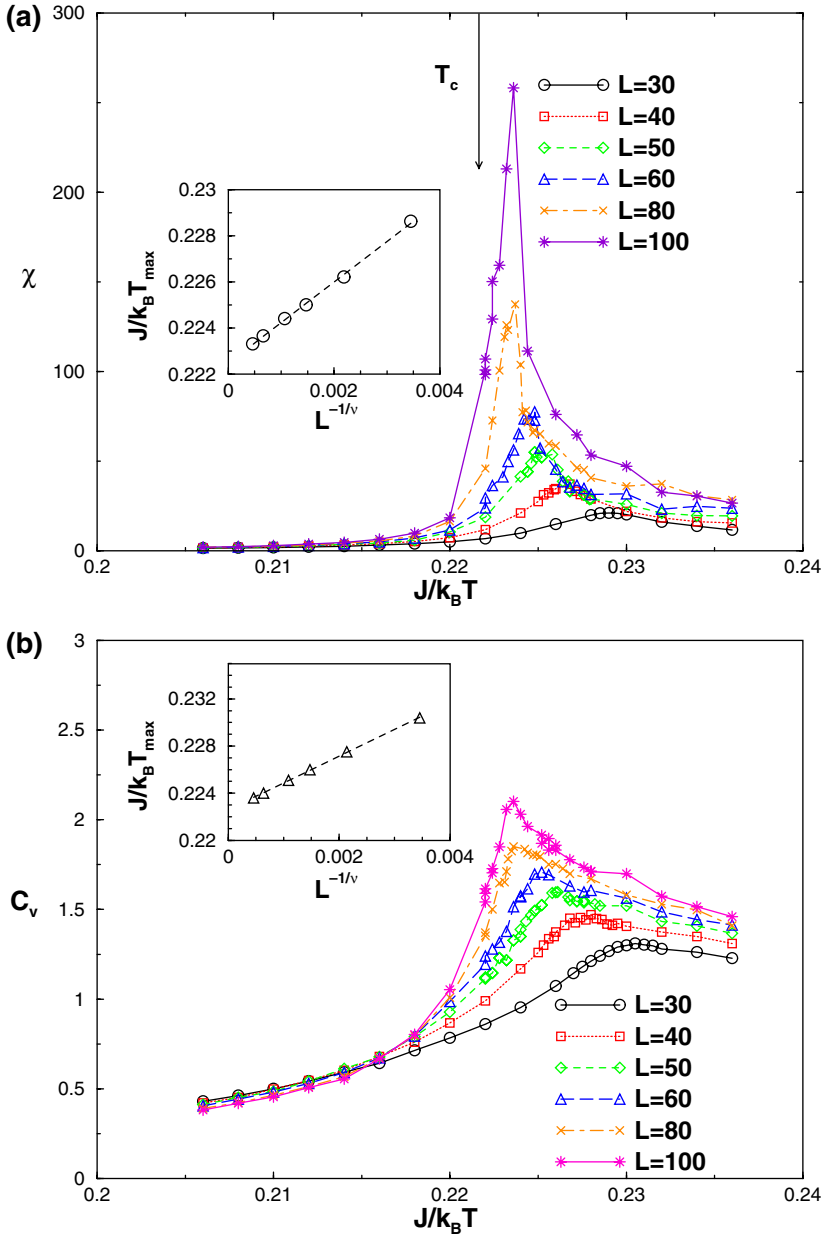


**Figure 7.** Susceptibility $\chi'$ (a) and specific heat $C_v$ (b) plotted versus inverse temperature, for $H_s = -2$ and various values of $L$, as shown by the key in the figure. The arrow shows the location of the bulk critical point. The insets show plots of the peak position versus $L^{-1/\nu}$.

$L = 20$–$160$. Thus, despite its simplifications, we feel that the simple theory of section 2 does provide a satisfactory description of the interfacial behaviour of our model.

We now turn to a description of the phase transition of our system with the choice of boundary condition as sketched in figure 2. Standard indicators of phase transitions in Ising systems are susceptibility $\chi'$ and specific heat $C_v$ (figure 7). While the shapes of these peaks

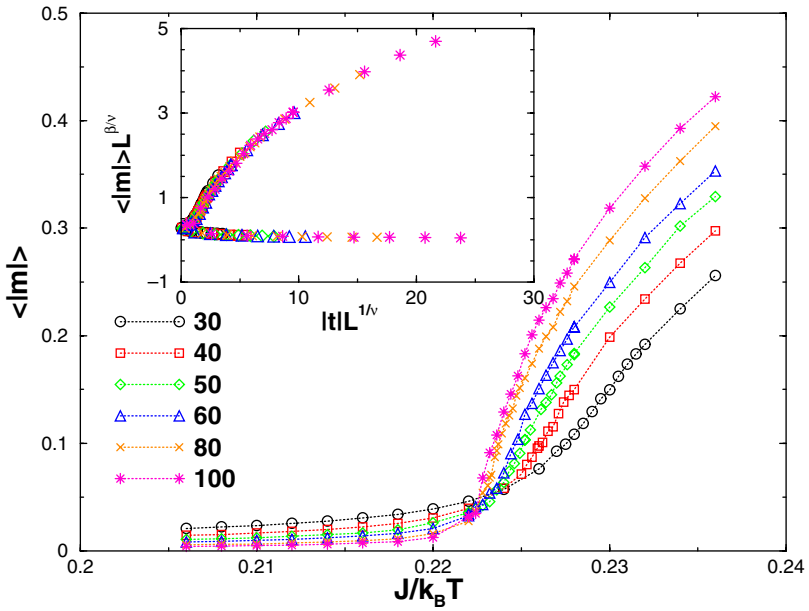


**Figure 8.** Plot of the order parameter $\langle|m|\rangle$ versus inverse temperature $J/k_{\mathrm{B}}T$, for various values of $L$ as shown in the key. Inset presents a corresponding finite size scaling representation, plotting $\langle|m|\rangle L^{\beta/\nu}$ versus $|t|L^{1/\nu}$.

look different from those found for systems with periodic boundary conditions, the qualitative behaviour is similar [59, 60]. In particular, the peak positions are roughly compatible with a simple linear variation

$$J/k_{\mathrm{B}}T_{\max} - J/k_{\mathrm{B}}T_{\mathrm{cb}} \propto L^{-1/\nu}. \tag{29}$$

Although, as pointed out in equation (27), a second scaling variable $H_{\mathrm{s}}L^{\Delta_1/\nu}$ is present, its effect on the location of the peak position of $\chi'$ seems to be relatively small.

A more pronounced change of behaviour is detected when we plot the order parameter $\langle|m|\rangle$ versus inverse temperature (figure 8): unlike the case of periodic boundary conditions (p.b.c.s), the curves for $\langle|m|\rangle$ versus $J/k_{\mathrm{B}}T$ intersect each other when $L$ is varied! For large $J/k_{\mathrm{B}}T$, $\langle|m|\rangle$ converges to $m_{\mathrm{b}}$ from below, while in the case of p.b.c.s exactly the opposite trend is observed. Note that for $L \leqslant 60$ in the shown temperature range the depression of $\langle|m|\rangle$ due to the boundary effects is rather dramatic. The intersections of the $\langle|m|\rangle$ versus $J/k_{\mathrm{B}}T$ curves for the various choices of $L$ *do not coincide precisely*, and there is also no theoretical reason why they should; but it is clear that for $L \to \infty$ these intersections must move towards $J/k_{\mathrm{B}}T_{\mathrm{cb}}$, and therefore the crowding of these intersection points for $J/k_{\mathrm{B}}T$ slightly exceeding $J/k_{\mathrm{B}}T_{\mathrm{cb}}$ is no surprise.

If one performs a finite size scaling analysis of $\langle|m|\rangle$ in the usual way [59, 60], plotting $\langle|m|\rangle L^{\beta/\nu}$ versus $|t|L^{1/\nu}$ (using the theoretical values of the Ising model exponents and the known value of $J/k_{\mathrm{B}}T_{\mathrm{cb}}$, as quoted above), one obtains a quite good data collapse, as the inset of figure 8 shows. Thus, despite the fact that the presence of the competing surface fields has changed the behaviour of $\langle|m|\rangle$ dramatically, and the theoretical arguments imply the presence of another scaling variable ($H_{\mathrm{s}}L^{\Delta_1/\nu}$ of equation (25)), which is not taken into account in the scaling plot shown in the inset of figure 8, one obtains rather nice scaling behaviour: the effect of the surface fields is somehow effectively absorbed in a different shape of the scaling

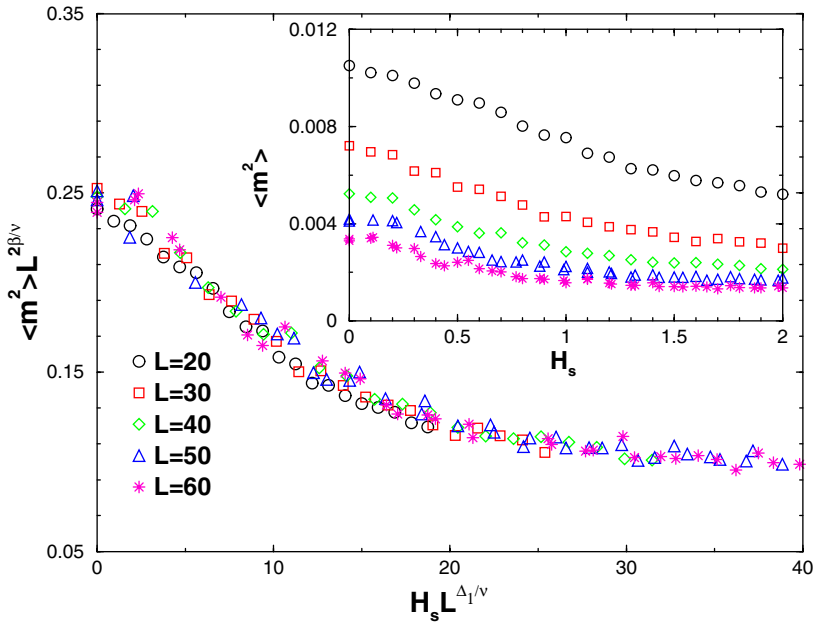


**Figure 9.** Plot of $\langle m^2 \rangle L^{2\beta/\nu}$ versus $H_s L^{\Delta_1/\nu}$, choosing $J/k_B T = J/k_B T_c = 0.2217$ and $20 \leqslant L \leqslant 60$, as indicated in the key. The inset shows the raw data $\langle m^2 \rangle$ versus $H_s$ used for this scaling plot.

function: this may be due to the fact that for the chosen value of $H_s$ one may replace the last argument $H_s L^{\Delta_1/\nu}$ in equations (24)–(26) effectively by its asymptotic value infinity.

To test this latter hypothesis, figure 9 analyses the behaviour of $\langle m^2 \rangle$ for $T = T_{cb}$ as a function of $H_s$. One sees that $\langle m^2 \rangle$ first decreases slowly and then reaches a limiting plateau (the earlier the larger $L$). The scaling plot $\langle m^2 \rangle L^{2\beta/\nu}$ versus $H_s L^{\Delta_1/\nu}$ again reveals reasonable data collapse; note that there are no adjustable parameters whatsoever. Moreover, for $H_s L^{\Delta_1/\nu} \geqslant 20$ the scaling function is indeed almost horizontal already, indicating that the above hypothesis that for $|H_s| = 2$ and $L \geqslant 30$ we may approximate $H_s L^{\Delta_1/\nu} \approx \infty$ is valid.

A consequence of the fact that (for $H = 0$) the moments $\langle |m|^k \rangle$ scale as

$$\langle |m|^k \rangle = L^{-k\beta/\nu} \tilde{m}^{(k)}(L^{1/\nu} t, H_s L^{\Delta_1/\nu}) \tag{30}$$

follows for the fourth order cumulant [62] $U_L = 1 - \langle m^4 \rangle / [3 \langle m^2 \rangle^2]$, which at $T_{cb}$ no longer is a 'universal' invariant (characteristic for a particular universality class, such as that of the three-dimensional Ising model, *and depends on the shape of the system and the boundary conditions used* [62, 63]).

Thus, from equation (30) we readily conclude

$$U_L(t = 0, H_s) = \tilde{U}(H_s L^{\Delta_1/\nu}), \qquad L \to \infty, |H_s| \to 0, \tag{31}$$

and the limits are taken such that $|H_s| L^{\Delta_1/\nu}$ remains finite.

The fact that we have identified two classes of universal behaviour, namely either free surfaces with no surface field ($H_s = 0$), or free surfaces with nonzero surface field (where the behaviour is controlled by the limit $|H| L^{\Delta_1/\nu} \to \infty$ which is reached for large $L$ irrespective of the precise value of $H_s$) shows that our choice of $|H_s| = 2$ in figures 5–8 is by no means too special. In contrast, this choice is very convenient since already in the range $30 \leqslant L \leqslant 100$ we

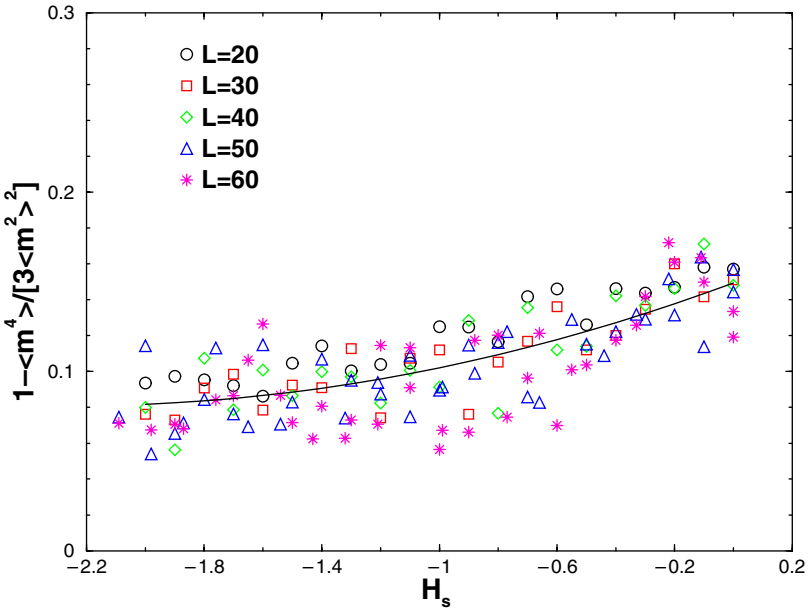


**Figure 10.** Cumulant $U_L = 1 - \langle m^4 \rangle / [3 \langle m^2 \rangle^2]$ at $T_{cb}$ plotted versus $H_s$ for various $L$, as indicated in the figure.

then already realize this limit, which for much smaller values of $|H_s|$ would only be reached for significantly larger systems.

We have attempted to estimate this fourth order cumulant (figure 10) but unfortunately due to its smallness (it decreases from about $\tilde{U}(0) \approx 0.14 \pm 0.02$ for $H_s = 0$, the case of free boundary conditions without surface fields [62], to a value $\tilde{U}(\infty) \approx 0.08 \pm 0.03$ for large values of $|H_s|$, see figure 10) it is rather difficult to obtain accurate estimates. The scatter seen in figure 10 indicates that the effort should be increased by about a factor of 100, in order to obtain a sufficient accuracy to verify the expected scaling behaviour. Since in view of figure 9, which verifies the scaling already for the second moment, there is no reason to doubt equation (31), we have not attempted to undergo such a huge computing effort, which needs substantial resources of computer time. In any case, figure 10 illustrates the fact that $U_L$ is very different in the present case from its value taken for periodic boundary conditions $\{U_L(T = T_{cb}) \approx 0.4656\}$.

## 4. Monte Carlo results: the two-dimensional case

The two-dimensional geometry has the merit that one can easily visualize the microstates of the system in terms of 'snapshot pictures' representing the spin configuration. Figure 11 presents two examples. One can see that at the temperatures shown the interface is a very contorted object, showing many overhangs particularly when $T \to T_{cb}$, and also large bubbles of the 'wrong' phase occur in the bulk. Obviously, for the temperatures shown one has to be careful with the predictions of the random walk model of the interface [55], and therefore we have not attempted to work out its predictions including precise quantitative detail.

Figure 12 considers the validity of equation (17), which for $p = 2$ can be written as

$$\ell(x) = A[(L/2 - x)^{1/2} + (L/2 + x)^{1/2}] - B, \tag{32}$$

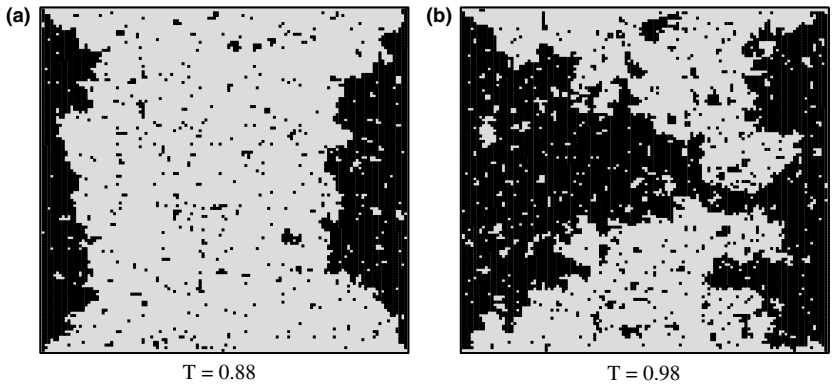


**Figure 11.** Snapshot pictures of the spin configuration of an $L \times L$ square lattice at $H_s = 2.0$ for $T = 0.88$ (a) and $T = 0.98$ (b), measuring temperatures in units of the critical temperature, for $L = 128$. Sites $i$ with $s_i = +1$ are shown in black, sites with $s_i = -1$ in light grey.

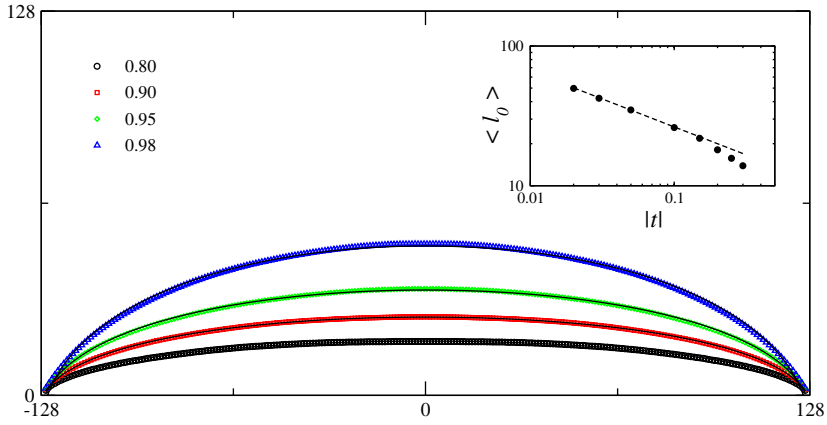


**Figure 12.** Plot of the average interface position $\ell(x)$ versus $x$ for the case $L = 256$ and four temperatures. The fit of equation (32) is indistinguishable from the actual data on the scale of this plot. The inset shows a log–log plot of $\ell_0$ versus $t$.

where the constants $A$, $B$ were treated as fit parameters. One finds that equation (32) is an excellent representation of the data, apart from the immediate vicinity of the corners, where $\ell(x) \to 0$ (these deviations cannot be resolved on the scale of the plot in figure 12).

It is also interesting to consider the temperature dependence of $\langle \ell_0 \rangle$ as $T_{cb}$ is approached. The empirical analysis suggests $\langle \ell_0 \rangle \propto t^{-0.4}$ (figure 12).

However, appealing to equation (16), which reduces for $p = 2$ to

$$\ell_0 \approx (2a/\sigma)^{1/4} L^{1/2}, \tag{33}$$

and noting that in the $d = 2$ Ising model $a = \frac{1}{2} k_B T a_0^2$ (equation (20)) and $\sigma \propto t$ [45–47], we would predict that for fixed (and large enough) $L$

$$\ell_0 \propto t^{-1/4}, \qquad t \to 0. \tag{34}$$

Actually, the log–log plot in figure 12 indicated some curvature, and thus it is possible that the asymptotic regime, where equation (34) holds, has not yet been reached. It is also

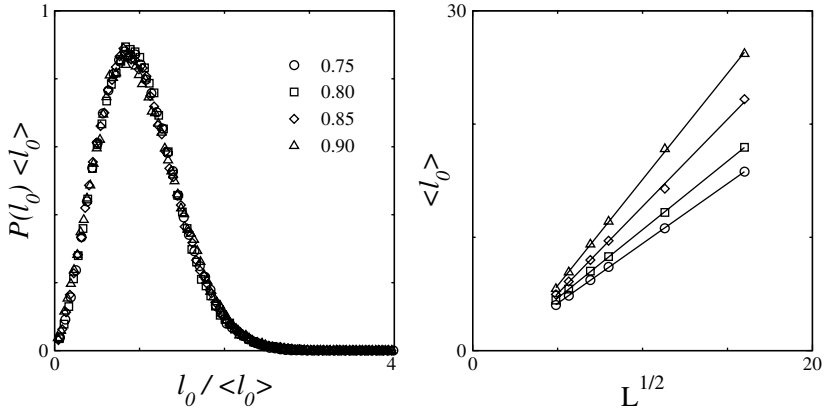


**Figure 13.** Scaled distribution $P(\ell_0)\langle\ell_0\rangle$ versus $\ell_0/\langle\ell_0\rangle$ for $L = 256$ and four temperatures $T = 0.75$, 0.80, 0.85 and 0.90 (left part) and variation of $\langle\ell_0\rangle$ with $L^{1/2}$ (right part).

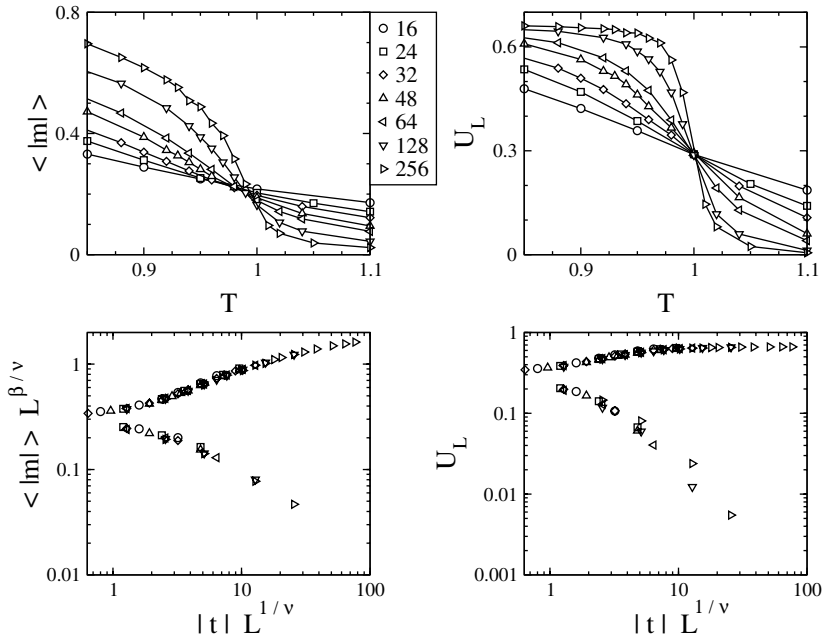


**Figure 14.** Plot of $\langle|m|\rangle$ versus $T$ and $U_L$ versus $T$, for Ising $L \times L$ squares with pairwise competing boundary fields of strength $H_s = 2$ (upper part) and corresponding finite site scaling plots (lower part). Linear dimensions from $L = 16$ to $L = 256$ are included.

possible that our data for $\ell_0$ very close to $T_{cb}$ are slightly 'contaminated' by finite size effects. Clearly, more work in the future will be required to resolve this issue.

Figure 13 shows the distribution of $\ell_0$ (left part) and the variation of $\langle\ell_0\rangle$ with $L$ (right part). It is seen that the behaviour $\ell_0 \propto L^{1/2}$ is nicely verified. All data refer to $H_s = 2.0$. Also the fact that $P(\ell_0)$ seems to be described by a universal distribution

$$P(\ell_0) = \frac{1}{\langle\ell_0\rangle}\tilde{P}(\ell_0/\langle\ell_0\rangle) \tag{35}$$

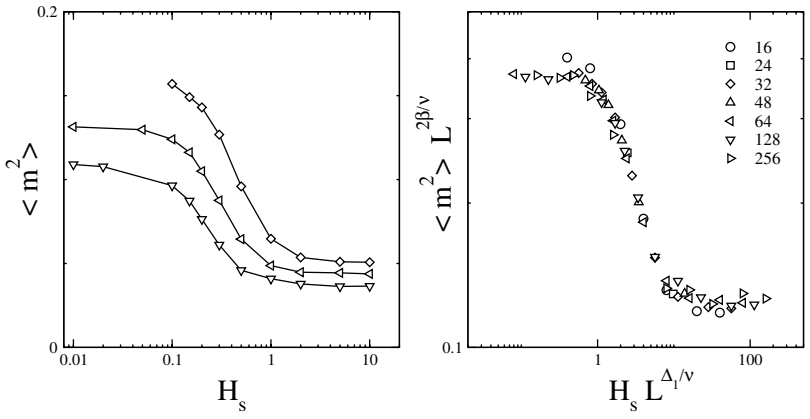


**Figure 15.** Plot of $\langle m^2 \rangle$ versus $H_s$ at $T = T_{cb}$, for three values of the linear dimension ($L = 32$, 64 and 128, from top to bottom), left part, and scaling plot $\langle m^2 \rangle L^{2\beta/\nu}$ versus $H_s L^{\Delta_1/\nu}$, right part, using the known values of the exponents for the two-dimensional Ising model ($\beta = 1/8$, $\Delta_1 = 1/2$, $\nu = 1$).

is interesting and should be further explored. It is remarkable that the width of $P(\ell_0)$ is comparable to $\langle \ell_0 \rangle$ itself. This is a typical property of distributions related to random walks, and hence we expect that equation (35) may be interpreted in terms of the random walk picture of interfaces in $d = 2$ Ising models [55].

Finally, we turn to the behaviour of the total magnetization $\langle |m| \rangle$ of the Ising square with these pairwise competing boundary fields, and related properties such as the second moment $\langle m^2 \rangle$ and the fourth order cumulant $U_L$ (figure 14). The picture is similar to the three-dimensional case: there is a strong depression of $\langle |m| \rangle$ for $T < T_{cb}$ for small $L$, in comparison to $m_b$, and magnetization curves for different $L$ intersect at temperatures slightly below $T_{cb}$; the cumulants $U_L$ do exhibit a unique intersection point at $T_{cb}$, but its value $\tilde{U}(\infty) \approx 0.3$ differs very strongly from the corresponding value for periodic boundary conditions (which is $U^* \approx 0.615$) [58–60]. Both $\langle |m| \rangle$ and $U_L$ show very good data collapse on the finite size scaling plots. Again the interpretation of these findings is that for $H_s = 2$ the scaling variable $H_s L^{\Delta_1/\nu} = H_s \sqrt{L}$ can already be replaced by its asymptotic value infinity, and the variation in the studied range (from $H_s \sqrt{L} = 8$ for $L = 16$ to $H_s \sqrt{L} = 32$ for $L = 256$) is not significant. Again this idea can be verified examining the variation of properties such as $\langle m^2 \rangle$ at $T_{cb}$ with $H_s$ (figure 15). One can see clearly that for $H_s L^{\Delta_1/\nu} \geqslant 20$ the asymptotic region, where no further change of $\langle m^2 \rangle L^{2\beta/\nu}$ with $H_s L^{\Delta_1/\nu}$ occurs, has been reached, and that this value is different from the value occurring for $H_s L^{\Delta_1/\nu} \ll 1$. A similar behaviour is also occurring for $\langle m^4 \rangle$, and for the cumulant $U_L$.

We finally turn to the prediction of equation (27) that an effective critical temperature $T_{c,L}$ of the finite system, defined e.g. from the temperature when the susceptibility $\chi'(T, H_s, L)$ has its maximum, should depend on the strength of the surface field, and so for fixed $L$ one finds a nontrivial curve in the plane of variables $(T, H_s)$ where this maximum occurs. Figure 16 shows three such curves $T_{c,L}(H_1)$ determined in this way. Of course, equation (27) implies that the corresponding scaled variable $|t|L^{1/\nu} = |1 - T_{c,L}(H_s)/T_{cb}|L^{1/\nu}$ is again a function of the scaled surface field $H_s L^{\Delta_1/\nu}$ only. The numerical data do confirm this prediction within some scatter. Again it is evident that for $H_s L^{\Delta_1/\nu} \geqslant 10$ there is little further change. As expected, the shift of $T_{c,L}$ for large $H_s$ (that means $H_s L^{\Delta_1/\nu} \geqslant 10$) is much larger than the shift of $T_{c,L}$ for small $H_s$ (that means $H_s L^{\Delta_1/\nu} \ll 1$), namely approximately four times larger.

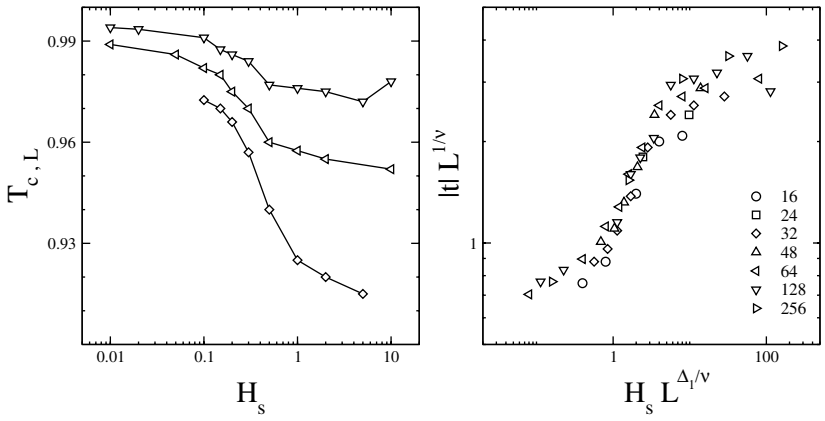


**Figure 16.** Plot of the effective critical temperature $T_{c,L}$ versus $H_s$ (note the logarithmic scale of the abscissa) for three choices of $L$ ($L = 128$, 64 and 32, from top to bottom), left part, and scaled shift of $T_c$ versus scaled surface field, including linear dimensions from $L = 16$ up to 256, as shown in the key. The known values of $T_{cb}$ and of the critical exponents ($\Delta_1 = 1/2$, $\nu = 1$) are used, so no adjustable parameters are present whatsoever. For further explanations, see the text.

## 5. Conclusions

In this paper, we have studied nearest neighbour Ising ferromagnets in $d = 2$ and 3 dimensions, assuming square and simple cubic lattices with free boundaries, and two pairs of boundaries on which surface fields of the same strength but opposite sign act ($\pm H_s$). Specifically, boundaries with the same orientation (along the $x$-axis or $xy$-plane, for instance) have the same sign of the surface field (figures 1(c), 2), so that the boundaries with the same sign of the surface field do not form a wedge ($d = 3$) or corner ($d = 2$), as shown in figure 1(b). It is shown that in the present case well below the bulk critical temperature $T_{cb}$ (but above the wetting transition temperature $T_w$) well defined precursors of wetting layers do occur for large linear dimension $L$ of the lattice (figures 1(c), 2(c), 3(d)), but unlike other choices for the arrangement of the competing surface fields (figures 1(a), (b)) no interface localization–delocalization transition distinct from the phase transition in the bulk occurs in the thermodynamic limit. Thus the transition that is observed for the present geometry presents nothing new with respect to bulk behaviour, but the finite size effects are quite different: the system develops near criticality states with a characteristic nonuniform magnetization distribution (figures 2(b), 3(b), (c), 4, 11, lower part), before the transition to configurations exhibiting the symmetry breaking (figures 2(c), 3(d), 11, upper part) gradually occurs. This behaviour has the consequence that the effective transition temperature $T_{c,L}$ (measured e.g. by the temperature where the susceptibility $\chi'$ of the finite system, equation (28), has its peak) is shifted to considerably lower value than would occur for systems without a boundary field (see e.g. figure 16). One also finds that the magnetization $\langle|m|\rangle$ is distinctly depressed relative to the corresponding bulk value $m_b$ (figures 8, 14), but standard finite size scaling, where $\langle|m|\rangle L^{\beta/\nu}$ is a simple function of $tL^{1/\nu}$ and $t = 1 - T/T_{cb}$, still holds if the surface field is sufficiently strong (i.e., $H_s L^{\Delta_1/\nu} \gg 1$). However, the scaling functions of magnetization (figures 8, 14) and other quantities, such as the fourth order cumulant (figure 14) in this limit clearly differ from their counterparts when no surface fields occur. We demonstrate that at the critical temperature the scaled moments of the distribution of the total magnetization in the system (figures 9 and 15) and the fourth order cumulant (figure 10) do depend on the value of the surface field. Thus,

even for $L \to \infty$ at $T = T_{cb}$ the surface field affects the 'bulk' behaviour of the system: of course, this observation is a simple corollary to the fact that a critical system where the correlation length is infinitely large is sensitive to boundary effects even if the boundaries are infinitely far away. Finite size scaling functions and related invariants, such as the value of the fourth order cumulant at $T_{cb}$, are not fully 'universal' but rather depend on the value of the scaling variable $H_s L^{\Delta_1/\nu}$. As a consequence, for $L \to \infty$ the fourth order cumulant for a system with free boundary conditions and fixed value of $H_s$ converges to two different values, depending on whether $H_s = 0$ or $H_s \neq 0$ (just as there are two distinct asymptotes in the plot for the second moment for small and large $H_s L^{\Delta_1/\nu}$, figure 15). Of course, one should recall that the finite size scaling functions (and the cumulant) also depend on the shape of the system (e.g., if we generalize from the $L \times L$ and $L \times L \times L$ geometries to rectangular $L \times M$ or $L \times L \times M$ shapes, with $M \neq L$) [63], but this problem has not been studied here.

An interesting finding concerns the precursors of the wetting layers formed in the region where $L$ by far exceeds the correlation length in the bulk. We have found that the interface separating these wetting layers from the majority domain has a characteristic shape (figures 5, 12), which can be accounted for (approximately) by a phenomenological theory based on the effective interface Hamiltonian (section 2). Simple approximate expressions for this interface contour $z = \ell(x)$ have been derived for both $d = 3$ (equation (9)) and $d = 2$ (equations (17), (32)) and found to be in fair agreement with observation (figures 5, 12). The maximum distance $\ell_0$ of this contour from the corresponding wall scales as $\ell_0 \propto \ln L$ ($(d = 3)$, equation (11)) or $\ell_0 \propto \sqrt{L}$ ($(d = 2)$, equations (16), (33)), again corroborated by the simulation (figures 6, 13). However, still more work is required to study the temperature dependence of this length $\ell_0$.

When one asks for real systems for which these findings are relevant, one should recall that Ising models can be re-interpreted as lattice gas models of fluids (spin down means a 'cell' is occupied by a fluid particle, spin up means the 'cell' is empty), and thus the present system could model a cavity (with linear dimensions in the nanometre or micrometre range) with inequivalent walls, such that one pair of opposing walls is wetted by the liquid, while the other pair is not. Of course, such a situation in practice will never correspond to the special case of precise antisymmetry of the surface fields $\pm H_s$, rather we expect a case where one pair of surfaces has a field $H_s$ and the other pair $-H_s'$, with $H_s < H_s'$, for instance. The behaviour studied here is then expected to occur when in addition a bulk field $H$ is present, of the order of $|H_s - H_s'|/L$, that effectively 'cancels' the difference between $H_s$ and $H_s'$, similar to the problem of capillary condensation (or evaporation, respectively) in thin films [6, 61]. The two-phase coexistence, as described in figures 1(c) and 2(c), is then expected to occur no longer at zero bulk field but at a field $H$ which is a nontrivial function of temperature, the difference $|H_s - H_s'|$, and $L$. While in our case the states in figure 2(c) possess a special symmetry (they can be transformed into each other by combining a flip of all spins with a rotation by 90°), this symmetry is lost. Of course, for real fluids there are additional complications due to a lack of symmetry between liquid and gas in the bulk, and due to the fact that the forces exerted from walls on the particles in a fluid typically are long range [1–5]. Similar complications occur when the Ising model is re-interpreted as a lattice model of a binary mixture (spin up represents an A particle, spin down a B particle). The present paper hence can only be a modest first step towards the understanding of real systems, which hence may exhibit a more complex behaviour than found here. We nevertheless hope that the present work will stimulate further interest in this problem and that experimentalists make efforts to test our predictions in real systems. We also suggest that the $d = 2$ case could also be theoretically studied with numerical variants of transfer matrix methods [64].

## Acknowledgments

The idea for this work originated from a very stimulating discussion with Professor Andrew Parry. We are very grateful for his interesting comments. One of us (ADV) thanks the DAAD for a fellowship and the Deutsche Forschungsgemeinschaft (DFG) for further support under grant number TR6/A5. AM thanks the DFG for support under grant number 436 BUL 113/130.

## References

[1] Sullivan D E and Telo da Gama M M 1986 *Fluid Interfacial Phenomena* ed C A Croxton (New York: Wiley) p 45
[2] de Gennes P G 1985 *Rev. Mod. Phys.* **57** 825
[3] Dietrich S 1988 *Phase Transitions and Critical Phenomena* vol 12, ed C Domb and J L Lebowitz (New York: Academic) p 1
[4] Schick M 1990 *Liquids at Interfaces* (*Les Houches Session XLVIII, 1988*) ed J Charvolin, J F Joanny and J Zinn-Justin (Amsterdam: Elsevier) p 415
[5] Parry A O 1996 *J. Phys.: Condens. Matter* **8** 10761
[6] Binder K, Landau D P and Müller M 2003 *J. Stat. Phys.* **110** 1411
[7] Concus P and Finn R 1969 *Proc. Natl Acad. Sci. USA* **63** 292
[8] Finn R 1986 *Equilibrium Capillary Surfaces* (Berlin: Springer)
[9] Pomeau Y 1986 *J. Colloid Interface Sci.* **113** 5
[10] Hauge E H 1992 *Phys. Rev.* A **46** 4994
[11] Rejmer K, Dietrich S and Napiorkowski M 1999 *Phys. Rev.* E **60** 4027
[12] Parry A O, Rascón C and Wood A J 1999 *Phys. Rev. Lett.* **83** 5535
[13] Rascón C and Parry A O 2000 *J. Chem. Phys.* **112** 5157
[14] Parry A O, Rascón C and Wood A J 2000 *Phys. Rev. Lett.* **85** 345
[15] Parry A O, Wood A J and Rascón C 2000 *J. Phys.: Condens. Matter* **12** 7671
[16] Parry A O, Wood A J and Rascón C 2001 *J. Phys.: Condens. Matter* **13** 4591
[17] Parry A O, Wood A J, Carlon E and Drzewinski A D 2001 *Phys. Rev. Lett.* **87** 196103
[18] Bednorz A and Napiorkowski M 2001 *J. Phys. A: Math. Gen.* **33** L353
[19] Parry A O, Greenall M J and Wood A J 2002 *J. Phys.: Condens. Matter* **14** 1169
[20] Jakubczyk P and Napiorkowski M 2002 *Phys. Rev.* E **66** 041107
[21] Abraham D B, Parry A O and Wood A J 2002 *Europhys. Lett.* **60** 106
[22] Abraham D B and Maciolek A 2002 *Phys. Rev. Lett.* **89** 286101
[23] Abraham D B, Mustonen V and Wood A J 2003 *Europhys. Lett.* **63** 408
[24] Albano E V, Heermann D W, Binder K and Paul W 1989 *Surf. Sci.* **223** 151
[25] Parry A O and Evans R 1990 *Phys. Rev. Lett.* **64** 439
[26] Parry A O and Evans R 1992 *Physica* A **181** 250
[27] Binder K, Landau D P and Ferrenberg A M 1995 *Phys. Rev. Lett.* **74** 298
[28] Binder K, Landau D P and Ferrenberg A M 1995 *Phys. Rev.* E **51** 2823
[29] Binder K, Evan R, Landau D P and Ferrenberg A M 1996 *Phys. Rev.* E **53** 5023
[30] Müller M and Binder K 2001 *Phys. Rev.* E **63** 021602
[31] Albano E V, De Virgiliis A, Müller M and Binder K 2003 *J. Phys.: Condens. Matter* **15** 333
[32] Milchev A, Müller M, Binder K and Landau D P 2003 *Phys. Rev. Lett.* **90** 136101
[33] Milchev A, Müller M, Binder K and Landau D P 2003 *Phys. Rev.* E **68** 031601
[34] Milchev A, Müller M and Binder K 2005 *Europhys. Lett.* **70** 348
[35] Milchev A, Müller M and Binder K 2005 *Phys. Rev.* E **72** 031603
[36] Müller M and Binder K 2005 *J. Phys.: Condens. Matter* **17** S333
[37] Schulz B J, Binder K and Müller M 2005 *Phys. Rev.* E **71** 046705
[38] Rockford L, Liu Y and Russel T P 1999 *Phys. Rev. Lett.* **82** 2602
[39] Rehse N, Wang C, Hund M, Geoghegan M, Magerle R and Krausch G 2001 *Eur. Phys. J.* E **4** 69
[40] Geoghegan M, Wang C, Rehse N, Magerle R and Krausch G 2005 *J. Phys.: Condens. Matter* **17** S389
[41] Champion Y and Fecht H J (ed) 2004 *Nano-Architechtured and Nano-Structured Materials* (Weinheim: Wiley–VCH)
[42] Binder K and Hohenberg P C 1972 *Phys. Rev.* B **6** 3461
[43] Binder K 1986 *Phase Transitions and Critical Phenomena* vol 8, ed C Domb and J L Lebowitz (New York: Academic)

[44] Diehl H W 1986 *Phase Transitions and Critical Phenomena* vol 10, ed C Domb and J L Lebowitz (New York: Academic)
[45] Widom B J 1972 *Phase Transitions and Critical Phenomena* vol 2, ed C Domb and M S Green (New York: Academic)
[46] Rowlinson J S and Widom B 1982 *Molecular Theory of Capillarity* (Oxford: Clarendon)
[47] Jasnow D 1984 *Rep. Prog. Phys.* **47** 1059
[48] Binder K and Müller M 2000 *Int. J. Mod. Phys.* C **11** 1093
[49] Indekeu J O 1994 *Int. J. Mod. Phys.* B **138** 309
[50] Koch W, Dietrich S and Napiorkowski M 1995 *Phys. Rev.* E **51** 3300
[51] Drelich J 1996 *Colloids Surf.* A **116** 43
[52] Getta T and Dietrich S 1998 *Phys. Rev.* E **57** 655
[53] Bauer C and Dietrich S 1999 *Eur. Phys. J.* B **10** 767
[54] Kroll D M and Gompper G 1989 *Phys. Rev.* B **39** 433
[55] Fisher M E 1984 *J. Stat. Phys.* **34** 667
[56] Fisher M E 1974 *Rev. Mod. Phys.* **46** 587
[57] Zinn-Justin J 2001 *Phys. Rep.* **344** 159
[58] Binder K and Luijten E 2001 *Phys. Rep.* **344** 179
[59] Binder K and Heermann D W 2002 *Monte Carlo Simulation in Statistical Physics. An Introduction* 4th edn (Berlin: Springer)
[60] Landau D P and Binder K 2005 *A Guide to Monte Carlo Simulation in Statistical Physics* 2nd edn (Cambridge: Cambridge University Press)
[61] Dillmann O, Janke W, Müller M and Binder K 2001 *J. Chem. Phys.* **114** 5853
[62] Binder K 1981 *Z. Phys.* B **43** 119
[63] Binder K and Wang J S 1989 *J. Stat. Phys.* **55** 87
[64] Stecki J 1993 *Phys. Rev.* **47** 7519
Stecki J, Maciolek A and Olausen K 1994 *Phys. Rev.* B **49** 1092
Maciolek A and Stecki J 1996 *Phys. Rev.* B **54** 1128
Maciolek A 1996 *J. Phys. A: Math. Gen.* **29** 3837
Carlon E and Drzewinksi A 1998 *Phys. Rev.* E **57** 2626